Chart III

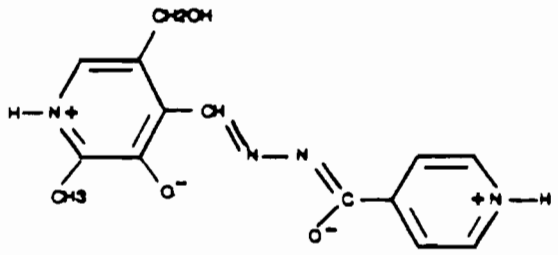

reaction 4, Table I) and that of the pyridinium (pK_1 = 2.26, reaction 1, Table I)). This is quite unlikely, because of the large difference between pK_4 and pK_1 (about 8). Additionally, in PBH, the isonicotinoyl is replaced by a benzoyl, which prevents the hydrazide–pyridine prototautomerism and would, therefore, lead to a less stable complex with iron. Nonetheless, affinity constants of PIH and PBH for Fe(II) are of the same order of magnitude (Table IV). This indicates that with Fe(II), in both complexes, PIH and PBH have a similar tridentate configuration which excludes the existence of a hydrazide–pyridine zwitterion in the Fe(II)–PIH complex. Therefore, the isonicotinoyl is probably engaged in the $Fe^{II}(PIH)_2$ complex in a neutral nonzwitterionic configuration. This analysis does not apply to SIH for which the difference between the pK of pyridine protonation (pK_3 = 3.33, Table I) and that of phenolate protonation (pK_4 = 8.30) is about 5. This can lead to a zwitterion with a stability range in the pH 6 region and which can be involved in complex formation. This zwitterion cannot, of course, occur with SBH, which can explain the lower affinity of the latter for iron as compared to that of SIH (Table IV). As for the pyridoxal moiety in neutral aqueous media, it is zwitterionic[11,12] and is probably directly involved in the Fe(II) and Fe(III) complexes with PIH and PBH. This can also explain the higher stabilities of these complexes as compared to those of SIH and SBH.

Affinity of PIH, PBH, SIH, and SBH for Fe(II) and Efficiency in Its Mobilization. Concluding Remarks. Iron is usually transported into the cell by the interaction of transferrin with a specific receptor situated in the plasma membrane and by the formation of a lipid vesicle containing both receptor and transferrin which is internalized in the cell.[13,14] After internalization of $(Fe^{3+})_2$–transferrin, iron is released within acidic vesicles, and the iron-depleted protein is recycled back to the plasma membrane.[13,14] It is strongly supported that iron mobilization from transferrin occurs according to four sequential steps: (1) acidification of the Fe^{III}_2–transferrin-containing endocytic vesicles; (2) enzymic reduction of Fe(III) to Fe(II); (3) movement of Fe(II) through the membrane by a concentration gradient process; (4) chelation of Fe(II) by cytoplasmic carriers.[14] Ponka et al. also estimated that Fe(III) is reduced before complex formation with PIH and that the removal of the complex from the cell is a very slow process which probably limits the efficiency of the chelate in iron mobilization.[2] However, in view of the complexity of the living cell, and even if iron is reduced into Fe(II) prior to complex formation and removal, we cannot expect a direct correlation between the ability of the chelating ligands to mobilize iron in vivo[6] and their affinity for Fe(II) (Table IV). In this process affinity is one factor among others which need to be investigated further, mostly from a biological standpoint.

Acknowledgment. We are grateful to Drs. J. Lomas and P. Fellman for constructive discussions and to Professors P. Ponka and H. M. Schulman for providing us with the chelating ligands.

Registry No. PIH, 737-86-0; PBH, 72343-06-7; SIH, 495-84-1; SBH, 3232-37-9; Fe, 7439-89-6.

Contribution from the Departments of Chemistry, State University of New York at Buffalo, Buffalo, New York 14214, and State University of New York, College at Fredonia, Fredonia, New York, 14603

Characterization of Protonated *trans*-Bis(dioxime)ruthenium Complexes: Crystal Structures of *trans*-Ru(DPGH)$_2$(NO)Cl, *trans*-[Ru(DMGH)(DMGH$_2$)(NO)Cl]Cl, and *trans*-Ru(DMGH)$_2$(NO)Cl

Lisa F. Szczepura,† James G. Muller,† Carol A. Bessel,† Ronald F. See,† Thomas S. Janik,‡ Melvyn Rowen Churchill,*,† and Kenneth J. Takeuchi*,†

Received November 8, 1991

Single-crystal X-ray diffraction studies were carried out on *trans*-Ru(DPGH)$_2$(NO)Cl (**1**), *trans*-[Ru(DMGH)(DMGH$_2$)(NO)Cl]Cl (**2**), and *trans*-Ru(DMGH)$_2$(NO)Cl (**3**) (DMGH = dimethylglyoxime monoanion, DPGH = diphenylglyoxime monoanion). These represent the first crystal structures of *trans*-bis(dioxime) complexes containing ruthenium. Complex **1** crystallizes in the monoclinic space group $C2/c$, with a = 10.459 (5) Å, b = 10.148 (4) Å, c = 26.673 (13) Å, β = 98.25 (4) Å, Z = 4, V = 2802 (2) Å^3, and R = 4.83%. Complex **2** crystallizes in the monoclinic space group $P2_1/c$, with a = 13.8100 (10) Å, b = 10.095 (2) Å, c = 11.898 (2) Å, β = 100.780 (10) Å, Z = 4, V = 1629.4 (4) Å^3, and R = 3.05%. Complex **3** crystallizes in the orthorhombic space group $P2_12_12_1$, with a = 7.9920 (10) Å, b = 14.251 (2) Å, c = 24.666 (2) Å, Z = 8, V = 2809.1 (5) Å^3, and R = 3.84%. The crystal structure determinations include the location and refinement of hydrogen atoms associated with the oxime oxygens. The existence of two types of hydrogen bonds (O–H--Cl hydrogen bonds and a symmetric O–H--O oxime bridge) associated with the oxime oxygen atoms of *trans*-[Ru(DMGH)(DMGH$_2$)(NO)Cl]Cl can be clearly demonstrated. Furthermore, the crystal structures of both *trans*-Ru(DPGH)$_2$(NO)Cl and *trans*-Ru(DMGH)$_2$(NO)Cl display a third type of hydrogen bonding (asymmetric O–H--O oxime bridge) involving the oxime oxygen atoms. Thus, three types of hydrogen bonding that were previously proposed for *trans*-bis(dioxime) transition metal complexes can be directly observed within these three structurally similar bis(dioxime)ruthenium complexes. In addition, we can now unambiguously assign the O–H stretching IR bands to the proper modes of hydrogen bridging. Temperature-dependent ^{1}H NMR spectroscopy of *trans*-[Ru(DMGH)(DMGH$_2$)(NO)Cl]Cl was used to measure rate constants of proton exchange, which demonstrated that the solid-state structure is maintained in solution. Finally, the cyclic voltammograms of complexes **2** and **3** and the pK_a values for the stepwise removal of two protons from complex **2** were measured.

Introduction

The coordination chemistry of *trans*-bis(dioxime) transition metal complexes continues to attract considerable attention as models of vitamin B_{12},[1] dioxygen carriers,[2] halogen atom abstraction agents[3] and catalysts in chemical processes.[4,5] In ad-

†State University of New York at Buffalo.
‡State University of New York, College at Fredonia.

(1) Pahor, N. B.; Dreos-Garlatti, R.; Geremia, S.; Randaccio, L.; Tauzher, G.; Zangrando, E. *Inorg. Chem.* **1990**, *29*, 3437–3441.
(2) Lance, K. A.; Goldsby, K. A.; Busch, D. H. *Inorg. Chem.* **1990**, *29*, 4537–4544.

0020-1669/92/1331-0859$03.00/0

dition, there is considerable interest in the role of protonation on the chemical reactivity of *trans*-bis(dioxime) transition metal complexes. Ligand substitution,[6] decomposition,[7] and alkyl-transfer reactions[8,9] of *trans*-bis(dioxime) transition metal complexes all display an acid dependence, where the rationale for acid dependence is proposed to be due to the protonation of the dioxime ligands. In particular, it has recently been demonstrated that *trans*-bis(dimethylglyoxime)ruthenium complexes act as catalysts in the oxidation of water and in the electrochemical epoxidation of olefins; the oxidizing ability of these complexes was found to be dependent on pH.[5] Thus, an unambiguous assignment of structural changes induced by dioxime protonation would be welcome from a functional as well as structural viewpoint.

Since the first report of a protonated *trans*-bis(dioxime) transition metal complex in 1923,[10] there have been conflicting proposals that the complex should be formulated as the acid salt *trans*-H[Co(DMGH)$_2$Cl$_2$] containing a lattice proton[11] or as *trans*-Co(DMGH)(DMGH$_2$)Cl$_2$ where the site of protonation is an oxime oxygen atom.[12] *trans*-Bis(dioxime) transition metal complexes usually exist in a macrocyclic configuration, where two intramolecular O–H--O hydrogen bridges link the two dioxime ligands, via the oxime oxygen atoms, into one macrocycle. However, these macrocyclic complexes can be protonated, which perturbs the structure and the function of the dioxime complex. The proponents of the theory involving the protonation of an oxime oxygen atom, first Wilkinson and later Crumbliss, have employed IR spectroscopy, as the primary means of characterization of protonated *trans*-bis(dioxime) transition metal complexes.[12-15] Crumbliss proposed that shifts in the absorbances due to O–H and N–O vibrations upon protonation result from the cleavage of one of the two intramolecular O–H--O hydrogen bridges and that the O–H--O cleavage results in the formation of free or intermolecularly hydrogen-bonded hydoxyl groups and the subsequent shortening of the second O–H--O hydrogen bridge.[13,14] These proposed structural changes from oxime protonation were somewhat substantiated by the X-ray single-crystal structure of [Co(DMGH)(DMGH$_2$)(C$_2$H$_5$)Cl]H$_2$O.[16] However, the assignment of IR absorbances and subsequent structural interpretations were complicated by the presence of a water of crystallization in the structure and by the lack of refinement of the bridging hydrogen atoms.

To the best of our knowledge, the only crystal structure reported of a protonated *trans*-bis(dioxime) transition metal complex in which the structural characterization included the refinement of hydrogen atoms is that of [Rh(DMGH)(DMGH$_2$)(P(C$_6$H$_5$)$_3$)Cl]Cl.[17] Protonation of *trans*-Rh(DMGH)$_2$(P(C$_6$H$_5$)$_3$)Cl was shown to occur at an oxime oxygen, breaking an O–H--O intramolecular hydrogen bond and causing a subsequent shortening of the second O–H--O hydrogen bridge. However, the infrared spectral data was not reported for this complex.

In order to clearly define the structural and physical properties associated with protonated *trans*-bis(dioxime) transition metal complexes, we report the X-ray single-crystal structures of *trans*-Ru(DPGH)$_2$(NO)Cl, *trans*-[Ru(DMGH)(DMGH$_2$)(NO)Cl]Cl, and *trans*-Ru(DMGH)$_2$(NO)Cl.[18] These represent the first structural characterizations of *trans*-bis(dioxime) complexes containing ruthenium, and all three structural determinations include refinements of the hydrogen atoms associated with the oxime oxygens. Thus, these crystal structures represent the first unambiguous structural demonstration of three types of hydrogen bridges between oxime atoms for structurally very similar transition metal dioxime complexes. In addition, we report the first structural characterization of a protonated *trans*-bis(dioxime) transition metal complex which is characterized by both X-ray diffraction (*including* the refinement of the hydrogen atoms) and IR spectroscopy. Because IR data has been linked to the structural characterization of transition metal bis(dioxime) complexes, our report, which combines both forms of characterization, is particularly important.

Temperature-dependent ^{1}H NMR spectroscopy of *trans*-[Ru(DMGH)(DMGH$_2$)(NO)Cl]Cl was used to measure rate constants of proton exchange. We observed that the solid-state structure is consistent with the solution proton exchange behavior. Also, the cyclic voltammograms of complexes **2** and **3** and the pK_a values for the subsequent removal of two protons from complex **2** were measured.

Experimental Section

Materials. Ruthenium trichloride trihydrate (obtained on loan from Johnson Matthey Inc.), dimethylglyoxime (Lancaster Synthesis Ltd.), and diphenylglyoxime (Aldrich Chemical Co.) were used as received. All solvents were of reagent grade and used as received.

Measurements. Elemental analyses were conducted by Atlantic Microlabs. Infrared spectra of Nujol mulls were measured with a Perkin-Elmer 710 B infrared spectrophotometer. ^{1}H NMR spectra were recorded using either a Varian EM-390 NMR spectrometer or a Varian VX-400 Fourier transform NMR spectrometer. Cyclic voltammetric experiments were carried out under a N_2 atmosphere using methylene chloride as the solvent and tetra-*n*-butylammonium tetrafluoroborate as the supporting electrolyte, which was prepared by standard methods.[19] A platinum working electrode (Bioanalytical Systems), a platinum auxiliary electrode, and a saturated sodium chloride calomel reference electrode (SSCE) were used for all electrochemical experiments. Prior to use the platinum working electrode was polished for 30 s utilizing a minimet polisher, 1 μm diamond polishing compound, metadi fluid, and polishing cloth (all obtained from Buehler Ltd., polishing cloth No. 40-7212), followed by sonication for 30 s in reagent grade methanol. Cyclic voltammetry was conducted with an IBM EC/225 polarographic analyzer equipped with a Houston Instruments Model 100 recorder.

Kinetic Measurements. ^{1}H NMR line shapes were calculated by using the program DNMR3.[20] The input parameters include line frequencies and corresponding line widths, relative intensities, values of the mean preexchange lifetime, and the exchange mechanism. T_2 values were calculated from the line widths at half-intensity taken from spectra under conditions of no exchange (T = −70 °C). Experimental spectra were compared directly with spectra calculated for various k (k = rate constant for proton exchange) values. The accuracy of the temperature was calculated to be ±3°.[21] Temperature dependence of the line frequencies was observed and corrected for by recording the slow-exchange spectra at various temperatures, determining the line dependence of the difference between the line frequencies ($\Delta\delta$) on temperature and correcting the input line frequencies accordingly.[22]

(3) Howes, K. R.; Bakac, A.; Espenson, J. H. *Inorg. Chem.* **1988**, *27*, 3147–3151.
(4) Kijma, M.; Miyamori, K.; Nakamura, T.; Sato, T. *Bull. Chem. Soc. Jpn.* **1990**, *63*, 2549–2554.
(5) (a) Taqui Khan, M. M.; Ramachandraiah, G.; Mehta, S. H.; Abdi, S. H. R.; Kumar, S. *J. Mol. Catal.* **1990**, *58*, 199–203. (b) Taqui Khan, M. M.; Ramachandraiah, G.; Mehta, S. H. *J. Mol. Catal.* **1989**, *50*, 123–129.
(6) Brown, K. L.; Tang, T. F. *Inorg. Chem.* **1987**, *26*, 3007–3022.
(7) Brown, K. T.; Ramamurthy, S.; Marynick, D. S. *J. Organomet. Chem.* **1985**, *287*, 377–394.
(8) Albey, P.; Dockal, E. R.; Halpern, J. *J. Am. Chem. Soc.* **1973**, *95*, 3166–3170.
(9) Adin, A.; Espenson, J. H. *J. Chem. Soc., Chem. Commun.* **1971**, 653–654.
(10) Feigel, F.; Rubinstein, H. *Justus Liebigs Ann. Chem.* **1923**, *433*, 183–190.
(11) Simonov, Y. A.; Dvorkin, A. A.; Bologa, O. A.; Ablov, A. V.; Minovskii, T. L. *Dokl. Akad. Nauk. SSR* **1973**, *210*, 433–435.
(12) Gillard, R. D.; Wilkinson, G. *J. Chem. Soc.* **1963**, 6041–6044.
(13) Crumbliss, A. L.; Gaus, P. L. *Inorg. Chem.* **1975**, *14*, 486–490.
(14) Crumbliss, A. L.; Gaus, P. L. *Inorg. Chem.* **1975**, *14*, 2745–2747.
(15) Gillard, R. D.; Osborn, J. A.; Wilkinson, G. *J. Chem. Soc.* **1965**, 1951–1965.
(16) Crumbliss, A. L.; Bowman, T.; Gaus, P. L.; McPhail, A. T. *J. Chem. Soc., Chem. Commun.* **1973**, 415–416.
(17) Villa, A. C.; Manfredotti, A. G.; Gaustini, C. *Cryst. Struct. Commun.* **1973**, *2*, 133–136.
(18) Muller, J. G.; Takeuchi, K. J. *Inorg. Chem.* **1990**, *29*, 2185–2188.
(19) Kissinger, P. T.; Heineman, W. *Laboratory Techniques in Electroanalytical Chemistry*; Dekker: New York, 1984.
(20) Kleier, D. A.; Binsch, G. DNMR3. A Computer Program for the Calculation of Complex Exchange-Broadened NMR Spectra. Modified Version for Spin Systems Exhibiting Magnetic Equivalence of Symmetry. *Quantum Chemistry Program Exchange*; Indiana University: Bloomington, IN, 1970; Program 165. Modified version by D. C. Roe (Du Pont Central Research) for use on a VAX computer and locally modified for use with DI-3000 graphics by J. B. Keister.
(21) Van Geet, A. L. *Anal. Chem.* **1970**, *42*, 679–680.
(22) Eliel, E. L.; Allinger, N. L. *Top. Stereochem.* **1968**, *3*, 97–192.

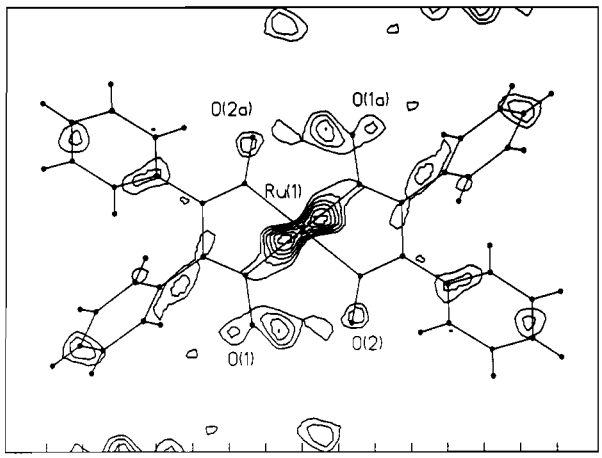

Figure 1. Difference electron-density map for *trans*-Ru(DPGH)$_2$(NO)Cl in the O(1)–O(2)–Ru(1)–O(2A)–O(1A) plane, showing the hydrogen atoms attached to O(1) and O(1A). Contours are at 0.1 e/Å^3, the lowest being at 0.1 e/Å^3.

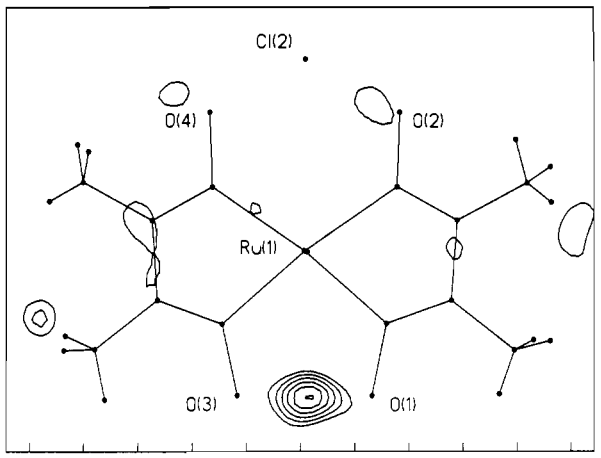

Figure 2. Difference electron-density map for *trans*-Ru(DMGH)(DMGH$_2$)(NO)Cl]Cl in the O(1)–Ru(1)–O(3) plane. The peak between from O(1) and O(3) indicates hydrogen bonding between O(1) and O(3) (Contours are as for Figure 1.)

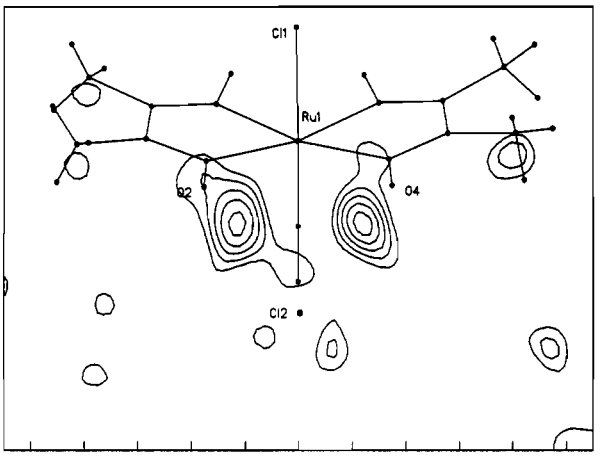

Figure 3. Difference electron-density map for *trans*-Ru(DMGH)(DMGH$_2$)(NO)Cl]Cl in the O(2)–Cl(2)–O(4) plane, showing the hydrogen bridging from DMGH$_2$ to Cl moiety.

Activation parameters were calculated from a least-squares determination of the slope and intercept of an Eyring plot of ln (k/T) vs $1/T$; error limits are given at the 95% confidence limits with use of Student's t values. It should be recognized that random errors in the experimental determinations of rate constants are expressed by the error limits of $\Delta H^{\ddagger}$ and $\Delta S^{\ddagger}$, but systematic errors due to, for example, incorrect estimates of line widths in the absence of exchange were not considered.

Potentiometric Titrations. The 0.001 M solutions of *trans*-[Ru(DMGH)(DMGH$_2$)(NO)Cl]Cl (**2**) and *trans*-[Ru(DMGH)$_2$(NO)Cl] (**3**) were prepared using distilled deaerated water and then titrated with 0.001 M NaOH at 15 and 25 °C, respectively, using an Orion Research Model 501 digital ionalyzer. Since the first end point was not well-defined in the titration of **2** the pK_a values were determined as follows. The volume at which the second endpoint was reached was determined from a plot of Δ^2(pH)/Δ^2V versus V (where V = volume of NaOH added). From this volume, the volumes at which the concentration of the given acid was equal to the concentration of its conjugate base was calculated and the pK_a values were determined. The pK_a of **3** was determined in a similar manner but the end point was determined from a plot of Δ(pH)/ΔV vs V. Three titrations were performed for each complex and average values reported.

Preparation of the Complexes. The complex *trans*-Ru(DPGH)$_2$(NO)Cl (**1**) was prepared as previously reported.[18]

***trans*-[Ru(DMGH)(DMGH$_2$)(NO)Cl]Cl, *trans*-Chloro(dimethylglyoximato)(dimethylglyoxime)(nitrosyl)ruthenium(II) Chloride (2).** This complex was prepared as previously described.[18] Single crystals were obtained by slow vapor diffusion from a methylene chloride/ethanol solution. Crystals were not exposed to heat or vacuum prior to characterization (including elemental analysis). Anal. Calcd for $C_8H_{15}Cl_2N_5O_5Ru$: C, 22.18; H, 3.49; Cl, 16.37. Found: C, 22.25; H, 3.45; Cl, 16.28. IR (Nujol mull): 2680 (O—H), 1895 (N≡O), 1615 (O—H--O), 1530 (C=N), 1235 and 1080 cm^{-1} (N—O) ^{1}H NMR (CD_2Cl_2, −70 °C): δ 2.4 (s, 6), 2.5 (s, 6), 12.9 (s, 2), 17.7 (s, 1). $E_{1/2}$ (CH_2Cl_2): −0.03, +1.55 (E_{pa}), and −0.88 (E_{pc}) V vs SSCE.

***trans*-Ru(DMGH)$_2$(NO)Cl, *trans*-Chlorobis(dimethylglyoximato)(nitrosyl)ruthenium(II) (3).** A 0.100-g sample of *trans*-[Ru(DMGH)(DMGH$_2$)(NO)Cl](Cl) (0.23 mmol) in 15 mL of acetone was stirred at room temperature for 10 min, and then 15 mL of H_2O was added. The existing red solution was then rotary evaporated until precipitation was observed. The mixture was cooled in an ice bath for 15 min. Red microcrystals were collected by vacuum filtration and washed with cold water; yield (0.080 g) 87%. Anal. Calcd for $C_8H_{14}ClN_5O_5Ru$: C, 24.22; H, 3.56; Cl, 8.93. Found: C, 24.48; H, 3.60; Cl, 8.86. IR (Nujol mull): 1860 (N≡O), 1505 (C=N), 1260 and 1080 cm^{-1} (N—O). ^{1}H NMR ($CDCl_3$): δ 2.4 (s, 12), 11.6 (s, 2). $E_{1/2}$ (CH_2Cl_2): −0.27, +1.41, and +1.17 (E_{pa}) V vs SSCE.

X-ray Structural Studies

A. Dark red single crystals of *trans*-Ru(DPGH)$_2$(NO)Cl (**1**) were obtained by slow vapor diffusion from an acetone/ethanol solution. The crystal selected for the structural study was mounted on a four-circle diffractometer (Syntex P2$_1$ upgraded to Siemens P3/V); appropriate crystallographic data are provided in Table I. The compound crystallizes in space group $C2/c$ with Z = 4; molecules have crystallographically imposed C_2 symmetry. The hydrogen atoms in the N–O–H portions of the DPGH ligands were located by difference-Fourier methods (see Figure 1) and were refined. Atomic coordinates are collected in Table II.

B. Orange-colored single crystals of *trans*-[Ru(DMGH)(DMGH$_2$)(NO)Cl]Cl (**2**) were obtained by slow vapor diffusion from a methylene chloride/ethanol solution. Details of data collection and structure solution are provided in Table I. This structure was both ordered and well-behaved under refinement. No crystallographic symmetry is imposed upon the molecule. (The compound crystallizes in space group $P2_1/c$, with Z = 4). Hydrogen atoms associated with the oxime portions of the DMGH and DMGH$_2$ ligands were located by difference-Fourier methods (see Figures 2 and 3) and were refined. Atomic coordinates are collected in Table III.

C. Deep red crystals of *trans*-Ru(DMGH)$_2$(NO)Cl (**3**) were obtained by slow vapor diffusion from an acetone/ethanol solution. Details of data collection and structure solution are listed in Table I. This compound crystallizes in the noncentrosymmetric space group $P2_12_12_1$ with Z = 8. The polarity of the crystal was correctly determined by "η-refinement", in which the parameter η is a multiplier of the $\Delta f''$ component of anomalous dispersion. The structure refined smoothly (to R = 3.84% for all data and R = 2.67% for data with $F > 6\sigma(F)$), and the hydrogen atoms of the oxime ligands were located by difference-Fourier methods (see Figure 4) and refined. Atomic coordinates are collected in Table IV. This structural study *does* present some problems. The crystallographic asymmetric unit contains two molecules of *trans*-Ru(DMGH)$_2$(NO)Cl. That defined by atoms labeled with a "B" suffix is ordered. The "A" molecule suffers from some form of disorder. The most obvious symptom is two sites for the oxygen atom of the nitrosyl ligand (O(5A) and O(6A)), but this is only the most obvious manifestation of the problem. The thermal parameters for most atoms in molecule A are substantially greater than those in molecule B; the effect seems concentrated in the y-direction (e.g., U_{22} for Ru(1A) = 0.101 (1) Å^2 versus U_{22} for Ru(1B) = 0.031 (1) Å^2, U_{22}[Cl(1A)] = 0.076 (1) Å^2 versus U_{22}[Cl(1B)] = 0.049 (1) Å^2, etc).

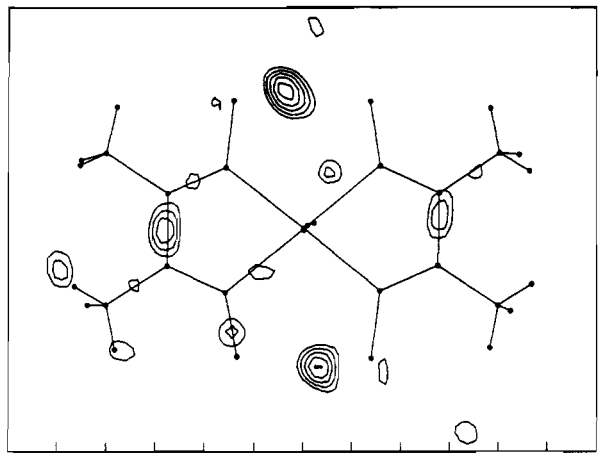

Figure 4. Difference electron-density map for $Ru(DMGH)_2(NO)Cl$. (Orientation and contours are as for Figure 1.)

Results and Discussion

Synthesis. The deprotonation of *trans*-[Ru(DMGH)-$(DMGH_2)$(NO)Cl]Cl (**2**) was accomplished by the addition of H_2O to an acetone solution of complex **2**, yielding an acidic (HCl) aqueous solution and *trans*-$Ru(DMGH)_2(NO)Cl$ (**3**). The deprotonation of complex **2** in aqueous solution is reminiscent of the reaction of cobaloxime complexes, where complete deprotonation was observed in aqueous solution.[13]

In an earlier report, we assigned the formulation of complex **2** as *trans*-$Ru(DMGH)_2(NO)Cl\cdot H_2O$.[18] In part, we proposed this formulation from the elemental analysis of complex **2**. On the basis of our present understanding of the acid/base chemistry of dioxime ligands, we can now reevaluate our original formulation. We have established that complex **2** can lose 1 equiv of HCl by heating at 80 °C under vacuum, resulting in the formation of complex **3**. Thus, since in our earlier report complex **2** was dried overnight in a vacuum oven at 80 °C prior to obtaining the elemental analysis, we propose that approximately 0.5 equiv of HCl was removed by vacuum, and thus the elemental analysis can be rationalized, for the calculated percent carbon and percent hydrogen values are close to the observed values, whether one H_2O or 0.5 HCl is used in the calculation. For this report, complex **2** was not dried in vacuo prior to elemental analysis; a satisfactory elemental analysis was obtained, where the analysis included a percent chlorine analysis.

Crystal Structures. Hydrogen atoms have been located and refined in each of the three structures that will be discussed. The electron density maps of Figures 1–4 show the evidence for the location of the hydrogen atoms associated with the glyoxime systems and the esd's on O–H distances (Tables V–VII) are those derived from least-squares refinement of the coordinates of the hydrogen atoms. Unfortunately, it must be borne in mind that (1) the hydrogen atom positions are known with very limited precision and (2) the O–H distances obtained are a measure of the distance between centroids of electron density and are not equivalent to internuclear distances. Thus, direct data on O–H distances must be used with the greatest care.

(A) *trans*-$Ru(DPGH)_2(NO)Cl$ (1). A general view of this molecule is provided in Figure 5. Interatomic distances and angles are collected in Table V. The structure is ordered and there are no abnormally short intermolecular contacts.

Molecules lie on sites of crystallographically-imposed C_2 symmetry, with the central ruthenium atom having a slightly distorted octahedral coordination geometry. The four equatorial nitrogen atoms of the DPGH ligands are coplanar to within ±0.02 Å and the ruthenium atom is displaced from this plane (toward the nitrosyl ligand) by 0.175 Å. The angle (α) between the planes of the two glyoxime ligands is 18.2°, while the N(1)–Ru(1)–N(2a) angle associated with the chelate ring is 77.6 (1)°.

The hydrogen atom of the glyoxime system was located and refined, yielding O(1)–H(1) = 0.79 (6) Å and O(2)···H(1) = 1.99 (6) Å [O(1)···O(2) = 2.743 (4) Å]. This suggests an O–H single bond with a very weak (if any) interaction between H(1) and O(2). The angle N(1)–O(1)–H(1) is 103 (4)°. The asymmetry of the O(1)–H(1)···O(2) system is carried back through the system. The N(1)–O(1) distance of 1.377 (5) Å is substantially longer than the N(2)–O(2) distance of 1.292 (5) Å, the N(1)–C(1) distance of 1.285 (5) Å is slightly shorter than the N(2a)–C(2) distance of 1.308 (5) Å, and the Ru(1)–N(1) distance of 2.008 (3) Å is significantly shorter than the Ru(1)–N(2) and Ru(1)–N(2a) distances of 2.050 (3) Å.

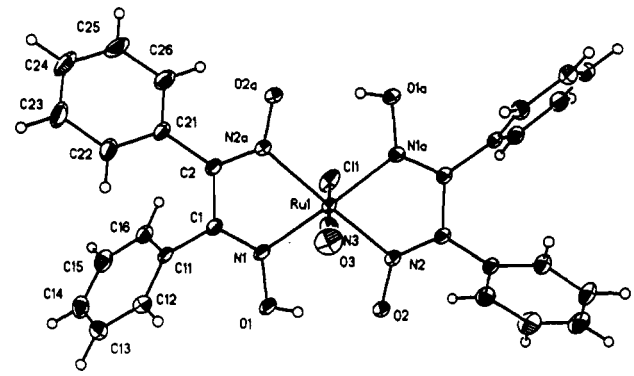

Figure 5. ORTEP2 view of *trans*-$Ru(DPGH)_2(NO)Cl$.

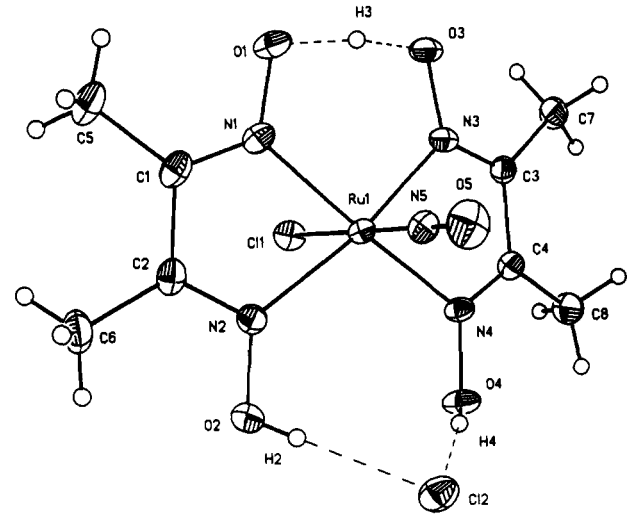

Figure 6. ORTEP2 view of *trans*-[Ru(DMGH)$(DMGH_2)$(NO)Cl]Cl.

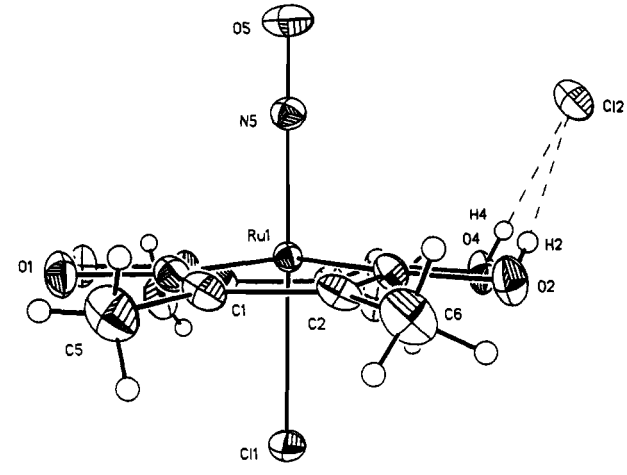

Figure 7. *trans*-[Ru(DMGH)$(DMGH_2)$(NO)Cl]Cl molecule with the Cl-Ru-NO axis vertical. Note the displacement of Ru(1) from the equatorial plane and the orientation of the O(2)–H(2)···Cl(2)···H(4)–O(4) bridge.

(B) *trans*-[Ru(DMGH)$(DMGH_2)$(NO)Cl]Cl (2). A general view of this molecule is shown in Figure 6, while Figure 7 shows

Table I. Experimental Data for the Crystallographic Studies of *trans*-Ru(DPGH)$_2$(NO)Cl (**1**), *trans*-[Ru(DMGH)(DMGH$_2$)(NO)Cl]Cl (**2**), and *trans*-Ru(DMGH)$_2$(NO)Cl (**3**)

	1	**2**[a]	**3**[a]
	Crystal Data		
empirical formula	$C_{28}H_{22}ClN_5O_5Ru$	$C_8H_{15}Cl_2N_5O_5Ru$	$C_8H_{14}ClN_5O_5Ru$
color and habit	bright red block	orange-red crystal	deep red crystal
cryst size, mm	0.30 × 0.30 × 0.30	0.40 × 0.30 × 0.12	0.40 × 0.30 × 0.25
cryst syst	monoclinic	monoclinic	orthorhombic
space group	$C2/c$ (No. 15)	$P2_1/c$ (No. 14)	$P2_12_12_1$ (No. 19)
a, Å	10.459 (5)	13.8100 (10)	7.9920 (10)
b, Å	10.148 (4)	10.095 (2)	14.251 (2)
c, Å	26.673 (13)	11.898 (2)	24.666 (2)
β, deg	98.25 (4)	100.780 (10)	
V, Å^3	2802 (2)	1629.4 (4)	2809.1 (5)
Z	4	4	8
fw	645.0	433.2	396.8
D(calcd), Mg/m^3	1.529	1.766	1.876
abs coeff, mm^{-1}	0.689	1.299	1.311
F(000)	1304	864	1584
	Data Collection		
diffractometer	Siemens $P2_1 \rightarrow P3/V$		
radiation	Mo Kα ($\bar{\lambda}$ = 0.71073 Å)		
T, K	296	296	295
monochromator	highly oriented graphite cryst		
2θ range, deg	6.0–50.0	8.0–50.0	8.0–50.0
scan type	ω	2θ–θ	ω
scan speed	constant; 2.00°/min in ω	constant; 1.50°/min in ω	constant; 2.49°/min in ω
scan range (ω), deg	0.95	0.70 plus Kα separation	0.70
bkgd meas	stationary cryst and stationary counter at beginning and end of scan, each for 25.0% of total scan time		
std reflcns	3 measd every 97 reflcns		
index ranges	$\lvert -12 \le h \le 0,\rvert$ $\lvert 0 \le k \le 12,\rvert$ $\lvert -31 \le l \le 31\rvert$	$\lvert 0 \le h \le 16,\rvert$ $\lvert -12 \le k \le 12,\rvert$ $\lvert -14 \le l \le 13\rvert$	$\lvert -9 \le h \le 0,\rvert$ $\lvert -16 \le k \le 16,\rvert$ $\lvert -29 \le l \le 29\rvert$
no. of reflcns collcd	2795	5993	10637
no. of indep reflcns	2482 (R_{int} = 1.65%)	2869 (R_{int} = 1.16%)	4957 (R_{int} = 1.23%)
no. of reflcns with $F > 6.0\sigma(F)$	1822	2277	3989
abs cor	semiempirical		
min/max transm	0.5088/0.6260	0.7094/1.0000	0.4682/0.5052
	Solution and Refinement		
syst	Siemens SHELXTL PLUS (VMS)		
solution	direct methods		
refin method	full-matrix least-squares		
quantity minimized	$\sum w(F_o - F_c)^2$	$\sum w(F_o - F_c)^2$	$\sum w(F_o - F_c)^2$
ext cor	b	χ = 0.000 60 (8), where $F^* = F\,[1 + 0.002\chi F^2/\sin(2\theta)]^{-1/4}$	b
hydrogen atoms	riding model, fixed isotropic U		
weighting scheme	$w^{-1} = \sigma^2(F) + 0.0033F^2$	$w^{-1} = \sigma^2(F) + 0.0002F^2$	$w^{-1} = \sigma^2(F) + 0.0003F^2$
number of params refined	187	251	371
final R indices ($F > 6.0\sigma(F)$)	R = 3.18%; R_w = 3.71%	R = 2.02%; R_w = 2.54%	R = 2.67%; R_w = 2.99%
R indices (all data)	R = 4.83%, R_w = 6.39%	R = 3.05%, R_w = 2.80%	R = 3.84%, R_w = 3.30%
goodness-of-fit	0.86	1.17	1.00
largest and mean Δ/σ	0.032, 0.004	0.021, 0.002	0.005, 0.000
data-to-param ratio	13.3:1	11.4:1	10.8:1
largest diff peak, e Å^{-3}	0.65	0.35	0.61

[a] A blank entry is the same as that for **1** unless otherwise indicated. [b] Not applied.

more clearly the juxtaposition of chloride ion and protonated glyoxime systems. Interatomic distances and angles are collected in Table VI. The structure consists of an ordered arrangement of [Ru(DMGH)(DMGH$_2$)(NO)Cl]$^+$ and Cl$^-$ ions which are held together by hydrogen bonds. The [Ru(DMGH)(DMGH$_2$)-(NO)Cl]$^+$ cations have approximate, but not exact, C_s symmetry (in the plane of Figure 7); the four equatorial nitrogen atoms are coplanar to within ±0.002 Å, while the octahedrally coordinated ruthenium atom is displaced out of plane (toward the nitrosyl ligand) by 0.155 Å. The angle between the planes of the glyoxime ligands (α) is 19.9°. The two independent chelate angles are N(1)–Ru(1)–N(2) = 76.0 (1)° and N(3)–Ru(1)–N(4) = 76.0 (1)°.

The O(1)···O(3) distance is 2.493 (3) Å with O(3)···H(3) = 1.07 (5) Å, O(1)···H(3)···O(3) = 169 (4)°; these data suggest hydrogen bonding between O(1) and O(3).

The chloride bridge between the dioxime systems is associated with an O(2)···O(4) distance of 3.521 (4) Å and localized O–H distances of O(2)–H(2) = 0.69 (3) Å and O(4)–H(4) = 0.73 (3) Å. Angles at the oxygen atoms are N(2)–O(2)–H(2) = 107 (3)° and N(4)–O(4)–H(4) = 107 (3)°.

The asymmetric opening of the two glyoxime systems is associated with the angles at ruthenium of N(1)–Ru(1)–N(3) = 96.6 (1) and N(2)–Ru(1)–N(4) = 110.1 (1)°.

The Ru–N bond lengths on the protonated (and chloride-bridged) site of the bis(glyoxime) system are Ru(1)–N(2) = 2.079 (2) Å and Ru(1)–N(4) = 2.079 (2) Å; these are significantly longer than those on the simple "hydrogen-bonded" side of the bis(glyoxime) system, where Ru(1)–N(1) = 2.028 (2) Å and Ru(1)–N(3) = 2.032 (2) Å. The N–O distances are longer on the diprotonated and chloride-bridged side of the molecule than on the hydrogen-bonded side, with N(2)–O(2) = 1.372 (4) Å and

Table II. Atomic Coordinates ($\times 10^4$) and Equivalent Isotropic Displacement Coefficients ($Å^2 \times 10^3$) for *trans*-Ru(DPGH)$_2$(NO)Cl (**1**)

	x	*y*	*z*	*U*
Ru(1)	0	4991 (1)	2500	31
Cl(1)	0	2716 (2)	2500	60
N(3)	0	6715 (5)	2500	41
O(3)	0	7832 (5)	2500	70
N(1)	1897 (3)	4838 (3)	2753 (1)	41
O(1)	2797 (3)	4771 (3)	2424 (1)	54
C(1)	2240 (4)	4630 (4)	3228 (1)	38
N(2)	−30 (3)	4801 (3)	1733 (1)	37
O(2)	1050 (3)	4827 (3)	1552 (1)	49
C(2)	1171 (4)	4642 (4)	3533 (1)	38
C(11)	3601 (3)	4345 (4)	3446 (1)	36
C(12)	4563 (4)	5250 (5)	3397 (2)	51
C(13)	5829 (5)	4968 (5)	3592 (2)	62
C(14)	6127 (4)	3772 (6)	3822 (2)	63
C(15)	5180 (4)	2869 (5)	3866 (2)	58
C(16)	3908 (4)	3157 (4)	3684 (1)	46
C(21)	1370 (4)	4443 (4)	4089 (1)	42
C(22)	2319 (5)	5152 (4)	4396 (2)	54
C(23)	2490 (7)	4994 (6)	4915 (2)	75
C(24)	1728 (6)	4123 (7)	5130 (2)	87
C(25)	804 (6)	3426 (6)	4834 (2)	81
C(26)	598 (5)	3581 (5)	4311 (2)	58
H(1)	2373 (52)	4872 (39)	2155 (23)	50
H(12A)	4351	6073	3228	80
H(13A)	6497	5603	3567	80
H(14A)	7008	3569	3954	80
H(15A)	5403	2031	4022	80
H(16A)	3240	2533	3726	80
H(22A)	2859	5757	4246	80
H(23A)	3144	5489	5124	80
H(24A)	1844	4011	5491	80
H(25A)	288	2810	4991	80
H(26A)	−76	3093	4110	80

[a] For non-hydrogen atoms *U* is the equivalent isotropic thermal parameter, defined as one-third of the trace of the orthogonalized U_{ij} tensor.

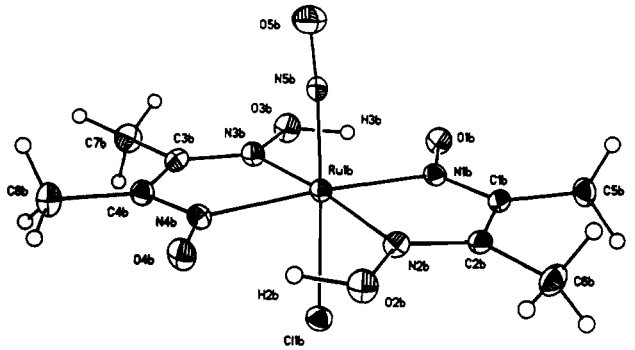

Figure 8. Molecule B of *trans*-Ru(DMGH)$_2$(NO)Cl.

N(4)–O(4) = 1.374 (3) Å as compared to N(1)–O(1) = 1.342 (3) Å and N(3)–O(3) = 1.333 (3) Å; the associated N–C distances show little difference.

(C) *trans*-Ru(DMGH)$_2$(NO)Cl (3). As discussed in the Experimental Section, this compound crystallizes with two molecules in the asymmetric unit. One (molecule B) is well-behaved and is illustrated in Figure 8. The other (molecule A) suffers from disorder. There are, presumably, two different orientations for the molecule at this location. Two individual peaks can be distinguished for the oxygen atom of the nitrosyl ligand, but the "vibration ellipsoids" of all atoms are somewhat misshapen (compare Figure 9 to Figure 8). A possible explanation (or partial explanation) is provided from a packing diagram which shows close contacts between the nitrosyl oxygen of molecule A and the chloride ligand of molecule B (see Figure 10). Rather surprisingly, most interatomic distances for molecules A and B show good agreement (see Table VII). In the subsequent discussion, however, we will refer to the more reliable values for molecule B.

Table III. Atomic Coordinates ($\times 10^4$) and Equivalent Isotropic Displacement Coefficients ($Å^2 \times 10^3$) for *trans*-[Ru(DMGH)(DMGH$_2$)(NO)Cl]Cl (**2**)

	x	*y*	*z*	*U*
Ru(1)	2520 (1)	518 (1)	2409 (1)	32
Cl(1)	1160 (1)	292 (1)	956 (1)	47
N(1)	2600 (2)	−1485 (2)	2333 (2)	43
C(1)	3045 (2)	−2022 (3)	1592 (3)	49
O(1)	2145 (2)	−2233 (2)	3009 (2)	57
N(2)	3352 (2)	171 (2)	1152 (2)	40
C(2)	3472 (2)	−1049 (3)	890 (2)	46
O(2)	3678 (2)	1093 (3)	460 (2)	60
N(3)	1530 (2)	594 (2)	3474 (2)	39
C(3)	1092 (2)	1702 (3)	3587 (2)	40
O(3)	1291 (2)	−513 (2)	3969 (2)	53
N(4)	2143 (2)	2511 (2)	2429 (2)	37
C(4)	1447 (2)	2806 (3)	2965 (2)	40
O(4)	2432 (2)	3511 (2)	1781 (2)	55
N(5)	3556 (2)	673 (2)	3509 (2)	42
O(5)	4224 (2)	768 (3)	4218 (2)	74
C(5)	3107 (4)	−3479 (4)	1443 (5)	71
C(6)	3992 (4)	−1469 (5)	−29 (4)	71
C(7)	282 (3)	1828 (4)	4247 (4)	61
C(8)	999 (3)	4146 (3)	2926 (4)	59
Cl(2)	4583 (1)	3204 (1)	2044 (1)	61
H(2)	3853 (26)	1627 (33)	803 (27)	54 (12)
H(3)	1680 (32)	−1297 (48)	3646 (37)	123 (16)
H(4)	2965 (25)	3483 (36)	1852 (29)	63 (12)
H(5A)	2846 (35)	−3663 (48)	748 (43)	117 (19)
H(5B)	2843 (45)	−3845 (62)	1954 (51)	160 (27)
H(5C)	3704 (38)	−3752 (49)	1458 (39)	117 (18)
H(6A)	3866 (32)	−810 (45)	−583 (36)	103 (17)
H(6B)	3770 (36)	−2106 (51)	−349 (38)	119 (19)
H(6C)	4644 (41)	−1444 (51)	103 (42)	140 (21)
H(7A)	−217 (39)	2260 (48)	3942 (38)	121 (20)
H(7B)	443 (30)	2310 (42)	4843 (34)	95 (14)
H(7C)	73 (35)	1040 (48)	4583 (39)	126 (17)
H(8A)	733 (37)	4341 (47)	3368 (43)	118 (19)
H(8B)	816 (33)	4403 (42)	2249 (43)	115 (18)
H(8C)	1611 (42)	4808 (55)	3144 (42)	146 (20)

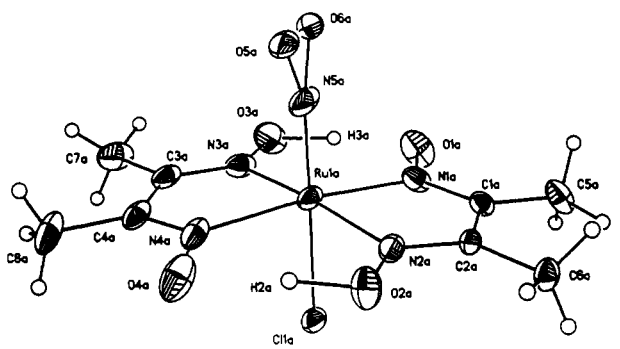

Figure 9. Molecule A of *trans*-Ru(DMGH)$_2$(NO)Cl. Note the disorder of the nitrosyl ligand and the larger thermal parameters (relative to Figure 8) of all other atoms.

As in the previous two structures, the ruthenium atom is in an octahedral coordination environment. The four equatorially-coordinated nitrogen atoms of the glyoxime ligands are coplanar to within ±0.014 Å, with the ruthenium atom being displaced from this plane (and toward the nitrosyl ligand) by 0.104 Å. The angle between the planes of the two glyoxime ligands (α) is 7.7°. The "chelate" angles for the five-membered ring are N(1b)–Ru(1b)–N(2b) = 77.7 (1)° and N(3b)–Ru(1b)–N(4b) = 77.7 (1)°.

Distances between the two glyoxime systems include O(1b)···O(3b) = 2.753 (5) Å and O(2b)···O(4b) = 2.793 (5) Å. The hydrogen atoms associated with these systems are situated such that on one side we have O(2b)–H(2b) = 1.02 (6) Å and O(4b)···H(2b) = 1.72 (8) Å with O(2b)–H(2b)···O(4b) = 165 (5)° and on the other side we have O(3b)–H(3b) = 1.06 (8) Å and O(1b)···H(3b) = 1.79 (6) Å with O(3b)–H(3b)···O(1b) = 163 (6)°. (We note that the disordered molecule A is associated with rather less symmetrical O···O contacts; this is probably a result of intermolecular hydrogen bonding—see Figure 10.)

Table IV. Atomic Coordinates ($\times 10^4$) and Equivalent Isotropic Displacement Coefficients ($Å^2 \times 10^3$) for *trans*-$Ru(DMGH)_2(NO)Cl$ (**3**)

	x	*y*	*z*	*U*
		Molecule A		
Ru(1A)	8870 (1)	5354 (1)	2522 (1)	55
Cl(1A)	7542 (2)	6018 (1)	3265 (1)	53
N(1A)	10604 (5)	6375 (3)	2619 (2)	58
O(1A)	10431 (5)	7206 (3)	2365 (2)	90
C(1A)	11841 (6)	6209 (3)	2954 (2)	43
N(2A)	10494 (5)	4769 (3)	3062 (2)	45
O(2A)	10260 (5)	3919 (3)	3262 (2)	66
C(2A)	11785 (5)	5271 (3)	3196 (2)	35
N(3A)	7151 (6)	6042 (5)	2065 (2)	72
O(3A)	7426 (6)	6915 (5)	1884 (2)	105
C(3A)	5760 (7)	5603 (6)	1967 (2)	70
N(4A)	6917 (5)	4423 (4)	2508 (2)	63
O(4A)	6929 (6)	3615 (3)	2784 (2)	88
C(4A)	5625 (7)	4666 (5)	2219 (2)	63
N(5A)	9832 (5)	4829 (6)	1965 (2)	93
O(5A)	10234 (22)	4228 (15)	1647 (8)	92
O(6A)	10580 (23)	4709 (15)	1548 (8)	92
C(5A)	13147 (7)	6898 (4)	3082 (3)	66
C(6A)	13132 (6)	4931 (3)	3568 (2)	49
C(7A)	4396 (8)	6036 (6)	1632 (3)	100
C(8A)	4169 (8)	4052 (5)	2150 (3)	88
H(2A)	9061 (140)	3554 (66)	3067 (42)	208 (46)
H(3A)	8615 (126)	7197 (56)	2042 (33)	138 (30)
H(5AA)	13886	6656	3356	80
H(5AB)	13790	7060	2767	80
H(5AC)	12626	7457	3219	80
H(6AA)	13030	5244	3912	80
H(6AB)	12956	4273	3629	80
H(6AC)	14216	5041	3413	80
H(7AA)	3436	6214	1842	80
H(7AB)	4783	6557	1419	80
H(7AC)	4030	5562	1382	80
H(8AA)	4301	3603	1863	80
H(8AB)	3854	3741	2480	80
H(8AC)	3248	4448	2051	80
		Molecule B		
Ru(1B)	7719 (1)	5052 (1)	−40 (1)	29
Cl(1B)	7241 (2)	4360 (1)	804 (1)	44
N(1B)	8751 (5)	3816 (3)	−288 (1)	33
O(1B)	10383 (4)	3698 (2)	−246 (1)	44
C(1B)	7732 (6)	3198 (3)	−487 (2)	34
N(2B)	5709 (4)	4331 (3)	−297 (2)	32
O(2B)	4129 (4)	4696 (3)	−275 (1)	46
C(2B)	5972 (6)	3500 (3)	−495 (2)	33
N(3B)	9698 (5)	5702 (3)	304 (2)	35
O(3B)	11261 (4)	5305 (3)	305 (1)	48
C(3B)	9437 (6)	6503 (3)	534 (2)	37
N(4B)	6659 (5)	6234 (3)	275 (1)	35
O(4B)	5054 (4)	6382 (2)	217 (2)	45
C(4B)	7695 (6)	6833 (3)	503 (2)	36
N(5B)	8054 (5)	5622 (2)	−659 (1)	32
O(5B)	8285 (5)	6040 (3)	−1043 (2)	62
C(5B)	8285 (7)	2273 (3)	−700 (2)	46
C(6B)	4589 (7)	2906 (3)	−725 (2)	47
C(7B)	10780 (7)	7047 (4)	804 (2)	53
C(8B)	7141 (7)	7768 (3)	700 (2)	53
H(2B)	4287 (68)	5360 (40)	−126 (22)	74 (18)
H(3B)	11115 (106)	4637 (54)	123 (30)	144 (29)
H(5BA)	9360	2112	−554	80
H(5BB)	7500	1793	−601	80
H(5BC)	8360	2305	−1088	80
H(6BA)	3540	3226	−685	80
H(6BB)	4779	2804	−1104	80
H(6BC)	4548	2314	−539	80
H(7BA)	11835	6887	642	80
H(7BB)	10593	7705	746	80
H(7BC)	10796	6910	1185	80
H(8BA)	7494	8262	461	80
H(8BB)	5945	7785	734	80
H(8BC)	7625	7876	1051	80

As with the other two structures, the equatorial Ru–N–O(–H) portions of the glyoxime systems show bond lengths in two distinct

Table V. Selected Interatomic Distances (Å) and Angles (deg) for *trans*-$Ru(DPGH)_2(NO)Cl$ (**1**)

(A) Ruthenium–Ligand and Nitrosyl N–O Distances

Ru(1)–Cl(1)	2.309 (2)	Ru–N(3)	1.749 (5)
Ru(1)–N(1)	2.008 (3)	Ru–N(1A)	2.008 (3)
Ru(1)–N(2)	2.050 (3)	Ru–N(2A)	2.050 (3)
N(3)–O(3)	1.134 (7)		

(B) Distances within the Glyoxime Ligand

N(1)–O(1)	1.377 (5)	O(1)–H(1)	0.794 (56)
N(2)–O(2)	1.292 (5)	N(1)–C(1)	1.285 (5)
N(2A)–C(2)	1.308 (5)	C(1)–C(2)	1.474 (6)
C(1)–C(11)	1.486 (5)	C(2)–C(21)	1.481 (5)

(C) Angles around the Ruthenium Atom

Cl(1)–Ru(1)–N(3)	180.0 (1)	Cl(1)–Ru(1)–N(1)	85.6 (1)
N(3)–Ru(1)–N(1)	94.4 (1)	Cl(1)–Ru(1)–N(2)	84.6 (1)
N(3)–Ru(1)–N(2)	95.4 (1)	N(1)–Ru(1)–N(2)	101.6 (1)
Cl(1)–Ru(1)–N(1A)	85.6 (1)	N(3)–Ru(1)–N(1A)	94.4 (1)
N(1)–Ru(1)–N(1A)	171.1 (2)	N(2)–Ru(1)–N(1A)	77.6 (1)
Cl(1)–Ru(1)–N(2A)	84.6 (1)	N(3)–Ru(1)–N(2A)	95.4 (1)
N(1)–Ru(1)–N(2A)	77.6 (1)	N(2)–Ru(1)–N(2A)	169.2 (2)
N(1A)–Ru(1)–N(2A)	101.6 (1)		

(D) Other Angles Involving Ruthenium

Ru(1)–N(1)–C(1)	117.8 (3)	Ru(1)–N(2)–C(2A)	115.8 (3)
Ru(1)–N(1)–O(1)	121.5 (2)	Ru(1)–N(2)–O(2)	118.9 (2)
Ru(1)–N(3)–O(3)	180.0		

(E) Other Angles within Glyoxime Systems

N(1)–O(1)–H(1)	103.0 (41)	O(1)–N(1)–C(1)	120.1 (3)
N(1)–C(1)–C(2)	114.6 (3)	C(1)–C(2)–N(2A)	114.0 (3)
O(2)–N(2)–C(2A)	125.3 (3)		

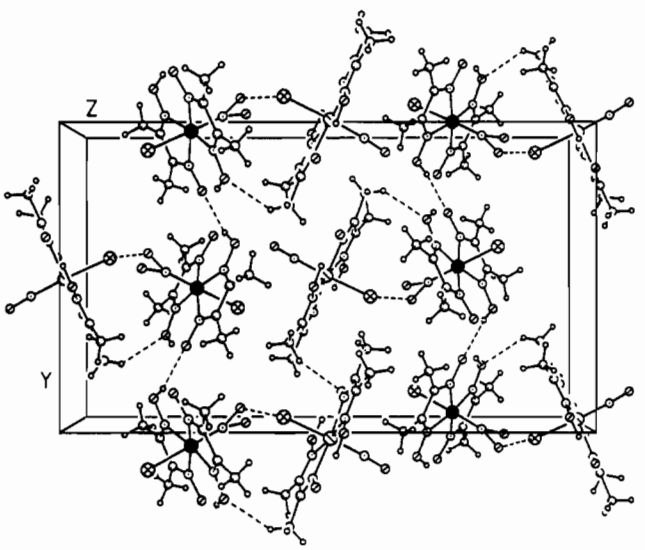

Figure 10. Packing diagram for *trans*-$Ru(DMGH)_2(NO)Cl$ showing close intermolecular interactions. The disordered molecules of type "A" have blackened Ru atoms. Note the contacts between disordered nitrosyl ligands (molecule A) and chloride ligands (molecule B) and also the intermolecular hydrogen bonding between the glyoxime systems of molecules A.

sets. Atoms N(2b) and N(3b) are associated with the protonated oxygen atoms; they are associated with longer N–O bonds and shorter Ru–N bonds than are the atoms N(1b) and N(4b) of the nonprotonated side of the ligands. Thus, N(2b)–O(2b) = 1.367 (5) Å and N(3b)–O(3b) = 1.372 (5) Å as compared to N(1b)–O(1b) = 1.319 (5) Å and N(4)–O(4b) = 1.308 (5) Å; also Ru(1b)–N(2b) = 2.010 (4) Å and Ru(1b)–N(3b) = 2.019 (4) Å as compared to Ru(1b)–N(1b) = 2.039 (4) Å and Ru(1b)–N(4b) = 2.039 (4) Å.

General Considerations. (1) The O–H--O Linkage between Glyoxime Ligands. The O---O distance between glyoxime ligands has been suggested by other researchers to be an indicator of the position of the hydrogen atom in the intramolecular bridge, although there are few previous examples of single-crystal structures of *trans*-bis(dioxime) complexes in which the hydrogen atoms have

Table VI. Selected Interatomic Distances (Å) and Angles (deg) for *trans*-[Ru(DMGH)(DMGH$_2$)(NO)Cl]Cl (**2**)

(A) Ruthenium–Ligand and Nitrosyl N–O Distances			
Ru(1)–Cl(1)	2.314 (1)	Ru(1)–N(1)	2.028 (2)
Ru(1)–N(2)	2.079 (2)	Ru(1)–N(3)	2.032 (2)
Ru(1)–N(4)	2.079 (2)	Ru(1)–N(5)	1.756 (2)
N(5)–O(5)	1.132 (3)		
(B) Distances within Glyoxime Ligands			
N(1)–C(1)	1.285 (4)	N(1)–O(1)	1.342 (3)
C(1)–C(2)	1.481 (4)	C(1)–C(5)	1.486 (5)
O(1)–H(3)	1.435 (48)	N(2)–C(2)	1.290 (4)
N(2)–O(2)	1.372 (4)	C(2)–C(6)	1.477 (6)
O(2)–H(2)	0.692 (32)	N(3)–C(3)	1.290 (3)
N(3)–O(3)	1.333 (3)	C(3)–C(4)	1.472 (4)
C(3)–C(7)	1.487 (6)	O(3)–H(3)	1.069 (48)
N(4)–C(4)	1.284 (4)	N(4)–O(4)	1.374 (3)
C(4)–C(8)	1.485 (5)	O(4)–H(4)	0.725 (34)
(C) Refined C–H (Methyl) Distances			
C(5)–H(5A)	0.859 (49)	C(5)–H(5B)	0.849 (67)
C(5)–H(5C)	0.867 (53)	C(6)–H(6A)	0.930 (44)
C(6)–H(6B)	0.780 (50)	C(6)–H(6C)	0.886 (56)
C(7)–H(7A)	0.839 (49)	C(7)–H(7B)	0.854 (40)
C(7)–H(7C)	0.959 (50)	C(8)–H(8A)	0.723 (55)
C(8)–H(8B)	0.839 (48)	C(8)–H(8C)	1.070 (54)
(D) Angles around the Ruthenium Atom			
Cl(1)–Ru(1)–N(1)	84.9 (1)	Cl(1)–Ru(1)–N(2)	85.8 (1)
N(1)–Ru(1)–N(2)	76.0 (1)	Cl(1)–Ru(1)–N(3)	85.6 (1)
N(1)–Ru(1)–N(3)	96.6 (1)	N(2)–Ru(1)–N(3)	169.1 (1)
Cl(1)–Ru(1)–N(4)	86.2 (1)	N(1)–Ru(1)–N(4)	168.9 (1)
N(2)–Ru(1)–N(4)	110.1 (1)	N(3)–Ru(1)–N(4)	76.0 (1)
Cl(1)–Ru(1)–N(5)	179.4 (1)	N(1)–Ru(1)–N(5)	94.5 (1)
N(2)–Ru(1)–N(5)	93.9 (1)	N(3)–Ru(1)–N(5)	94.7 (1)
N(4)–Ru(1)–N(5)	94.3 (1)		
(E) Other Angles			
Ru(1)–N(1)–O(1)	119.9 (2)	Ru(1)–N(1)–C(1)	119.2 (2)
N(1)–C(1)–C(2)	113.5 (3)	C(1)–N(1)–O(1)	120.8 (2)
C(2)–C(1)–C(5)	123.5 (3)	N(1)–C(1)–C(5)	123.0 (3)
Ru(1)–N(2)–C(2)	116.6 (2)	N(1)–O(1)–H(3)	104.6 (20)
C(2)–N(2)–O(2)	115.6 (2)	Ru(1)–N(2)–O(2)	127.2 (2)
C(1)–C(2)–C(6)	121.8 (3)	C(1)–C(2)–N(2)	114.5 (3)
N(2)–O(2)–H(2)	106.9 (30)	N(2)–C(2)–C(6)	123.7 (3)
Ru(1)–N(3)–O(3)	119.6 (2)	Ru(1)–N(3)–C(3)	118.8 (2)
N(3)–C(3)–C(4)	113.4 (2)	C(3)–N(3)–O(3)	121.4 (2)
C(4)–C(3)–C(7)	123.7 (3)	N(3)–C(3)–C(7)	122.9 (3)
Ru(1)–N(4)–C(4)	116.2 (2)	N(3)–O(3)–H(3)	106.2 (25)
C(4)–N(4)–O(4)	115.6 (2)	Ru(1)–N(4)–O(4)	127.2 (2)
C(3)–C(4)–C(8)	122.0 (3)	C(3)–C(4)–N(4)	115.2 (2)
N(4)–O(4)–H(4)	107.5 (28)	N(4)–C(4)–C(8)	122.8 (3)
O(1)–H(3)–O(3)	169.3 (41)	Ru(1)–N(5)–O(5)	179.7 (3)

been located.[17,23-25] Data obtained for complexes **1–3** are consistent with the proposed trend[23,26] that as the O···O distance increases above 2.4 Å, the hydrogen atom becomes unsymmetrically oriented between the two oxime oxygens at about 1 Å from one of the oxygen atoms.

The value obtained for the O···O distance associated with the intramolecular hydrogen bridge for complex **2** is substantially shorter than the values for complexes **1** and **3**. The decrease in the O···O distance is attributed to protonation of an oxime oxygen resulting in cleavage of one intramolecular hydrogen bridge and subsequent shortening of the opposite O(1)–O(3) distance to 2.493 (3) Å. The inequivalence of the two O···O distances (Δ = 1.028 Å) associated with complex **2** is consistent with the results obtained for protonated *trans*-bis(dioxime) complexes of other transition metals, viz. [Co(DMGH)(DMGH$_2$)(Et)Cl]H$_2$O[16] and [Rh(DMGH)(DMGH$_2$)(PPh$_3$)Cl]Cl.[17]

Table VII. Selected Bond Lengths (Å) and Angles (deg) for *trans*-Ru(DMGH)$_2$(NO)Cl (**3**)

Molecule B (ordered)		Molecule A (disordered?)	
(A) Ruthenium–Ligand and Nitrosyl N–O Distances			
Ru(1B)–Cl(1B)	2.333 (1)	Ru(1A)–Cl(1A)	2.320 (1)
Ru(1B)–N(1B)	2.039 (4)	Ru(1A)–N(1A)	2.024 (5)
Ru(1B)–N(2B)	2.010 (4)	Ru(1A)–N(2A)	2.039 (4)
Ru(1B)–N(3B)	2.019 (4)	Ru(1A)–N(3A)	2.029 (5)
Ru(1B)–N(4B)	2.039 (4)	Ru(1A)–N(4A)	2.049 (5)
Ru(1B)–N(5B)	1.750 (3)	Ru(1A)–N(5A)	1.742 (5)
N(5B)–O(5B)	1.134 (5)	N(5A)–O(5A)	1.207 (21)
		N(5A)–O(6A)	1.202 (20)
		O(5A)···O(6A)	0.779 (29)
(B) Distances within DMGH Ligands			
N(1B)–O(1B)	1.319 (5)	N(1A)–O(1A)	1.347 (7)
N(1B)–C(1B)	1.296 (6)	N(1A)–C(1A)	1.311 (6)
C(1B)–C(2B)	1.471 (7)	C(1A)–C(2A)	1.464 (7)
N(2B)–C(2B)	1.298 (6)	N(2A)–C(2A)	1.298 (6)
N(2B)–O(2B)	1.367 (5)	N(2A)–O(2A)	1.321 (6)
O(2B)–H(2B)	1.023 (56)	O(2A)–H(2A)	1.192 (112)
C(1B)–C(5B)	1.486 (6)	C(1A)–C(5A)	1.468 (7)
C(2B)–C(6B)	1.503 (7)	C(2A)–C(6A)	1.496 (6)
N(3B)–O(3B)	1.372 (5)	N(3A)–O(3A)	1.339 (10)
N(3B)–C(3B)	1.291 (6)	N(3A)–C(3A)	1.299 (8)
N(4B)–O(4B)	1.308 (5)	N(4A)–O(4A)	1.338 (7)
N(4B)–C(4B)	1.314 (6)	N(4A)–C(4A)	1.301 (7)
C(3B)–C(4B)	1.472 (7)	C(3A)–C(4A)	1.476 (10)
O(3B)–H(3B)	1.060 (79)	O(3A)–H(3A)	1.103 (93)
C(3B)–C(7B)	1.482 (7)	C(3A)–C(7A)	1.502 (9)
C(4B)–C(8B)	1.487 (6)	C(4A)–C(8A)	1.466 (9)
(C) Angles around Ruthenium and Nitrosyl Ligands			
Cl(1B)–Ru(1B)–N(1B)	88.2 (1)	Cl(1A)–Ru(1A)–N(1A)	85.8 (1)
N(1B)–Ru(1B)–N(2B)	77.7 (1)	N(1A)–Ru(1A)–N(2A)	77.3 (2)
N(1B)–Ru(1B)–N(3B)	101.8 (2)	N(1A)–Ru(1A)–N(3A)	100.5 (2)
Cl(1B)–Ru(1B)–N(4B)	86.7 (1)	Cl(1A)–Ru(1A)–N(4A)	85.9 (1)
N(2B)–Ru(1B)–N(4B)	102.2 (1)	N(2A)–Ru(1A)–N(4A)	103.4 (2)
Cl(1B)–Ru(1B)–N(5B)	177.3 (1)	Cl(1A)–Ru(1A)–N(5A)	178.5 (2)
N(2B)–Ru(1B)–N(5B)	94.8 (2)	N(2A)–Ru(1A)–N(5A)	93.4 (2)
N(4B)–Ru(1B)–N(5B)	90.7 (2)	N(4A)–Ru(1A)–N(5A)	92.6 (2)
Cl(1B)–Ru(1B)–N(2B)	86.3 (1)	Cl(1A)–Ru(1A)–N(2A)	86.6 (1)
Cl(1B)–Ru(1B)–N(3B)	87.0 (1)	Cl(1A)–Ru(1A)–N(3A)	86.1 (1)
N(2B)–Ru(1B)–N(3B)	173.3 (2)	N(2A)–Ru(1A)–N(3A)	172.5 (2)
N(1B)–Ru(1B)–N(4B)	174.9 (1)	N(1A)–Ru(1A)–N(4A)	171.6 (2)
N(3B)–Ru(1B)–N(4B)	77.7 (1)	N(3A)–Ru(1A)–N(4A)	77.8 (2)
N(1B)–Ru(1B)–N(5B)	94.4 (1)	N(1A)–Ru(1A)–N(5A)	95.7 (2)
N(3B)–Ru(1B)–N(5B)	91.9 (2)	N(3A)–Ru(1A)–N(5A)	93.9 (2)
Ru(1B)–N(5B)–O(5B)	175.9 (3)	Ru(1A)–N(5A)–O(5A)	159.3 (11)
		Ru(1A)–N(5A)–O(6A)	162.8 (12)
		O(5A)···N(5A)···O(6A)	37.7 (14)
(D) Other Angles			
Ru(1B)–N(1B)–O(1B)	119.1 (3)	Ru(1A)–N(1A)–O(1A)	120.5 (3)
O(1B)–N(1B)–C(1B)	124.3 (4)	O(1A)–N(1A)–C(1A)	122.0 (4)
N(1B)–C(1B)–C(5B)	123.4 (5)	N(1A)–C(1A)–C(5A)	123.5 (5)
Ru(1B)–N(2B)–O(2B)	122.1 (3)	Ru(1A)–N(2A)–O(2A)	121.9 (3)
O(2B)–N(2B)–C(2B)	120.8 (4)	O(2A)–N(2A)–C(2A)	121.5 (4)
C(1B)–C(2B)–N(2B)	114.6 (4)	C(1A)–C(2A)–N(2A)	115.1 (4)
N(2B)–C(2B)–C(6B)	122.5 (4)	N(2A)–C(2A)–C(6A)	123.4 (4)
Ru(1B)–N(3B)–C(3B)	117.6 (3)	Ru(1A)–N(3A)–C(3A)	116.7 (5)
N(3B)–O(3B)–H(3B)	105.7 (45)	N(3A)–O(3A)–H(3A)	111.3 (43)
N(3B)–C(3B)–C(7B)	122.9 (4)	N(3A)–C(3A)–C(7A)	121.7 (7)
Ru(1B)–N(4B)–O(4B)	119.9 (3)	Ru(1A)–N(4A)–O(4A)	122.9 (4)
O(4B)–N(4B)–C(4B)	124.0 (4)	O(4A)–N(4A)–C(4A)	120.9 (5)
C(3B)–C(4B)–C(8B)	123.4 (4)	C(3A)–C(4A)–C(8A)	123.3 (5)
Ru(1B)–N(1B)–C(1B)	116.5 (3)	Ru(1A)–N(1A)–C(1A)	117.5 (4)
N(1B)–C(1B)–C(2B)	114.0 (4)	N(1A)–C(1A)–C(2A)	113.5 (4)
C(2B)–C(1B)–C(5B)	122.6 (4)	C(2A)–C(1A)–C(5A)	123.0 (4)
Ru(1B)–N(2B)–C(2B)	117.1 (3)	Ru(1A)–N(2A)–C(2A)	116.5 (3)
N(2B)–O(2B)–H(2B)	104.6 (31)	N(2A)–O(2A)–H(2A)	111.3 (46)
C(1B)–C(2B)–C(6B)	122.9 (4)	C(1A)–C(2A)–C(6A)	121.5 (4)
Ru(1B)–N(3B)–O(3B)	121.7 (3)	Ru(1A)–N(3A)–O(3A)	121.5 (4)
O(3B)–N(3B)–C(3B)	120.7 (4)	O(3A)–N(3A)–C(3A)	121.8 (6)
N(3B)–C(3B)–C(4B)	114.3 (4)	N(3A)–C(3A)–C(4A)	114.9 (5)
C(4B)–C(3B)–C(7B)	122.8 (4)	C(4A)–C(3A)–C(7A)	123.4 (6)
Ru(1B)–N(4B)–C(4B)	115.9 (3)	Ru(1A)–N(4A)–C(4A)	116.2 (4)
C(3B)–C(4B)–N(4B)	114.3 (4)	C(3A)–C(4A)–N(4A)	114.4 (5)
N(4B)–C(4B)–C(8B)	122.3 (4)	N(4A)–C(4A)–C(8A)	122.3 (6)

(2) N–O(oxime) Bond Lengths. It has previously been observed for other *trans*-bis(dioxime) transition metal complexes that the N–O bond distances appear to be sensitive indicators of the position of the hydrogen atom between the oxygen atoms of the two oximes. Dissimilar N–O bond lengths imply that the proton lies closer to that oxygen atom which is associated with the longer

(23) Bowman, K.; Gaughan, A. P.; Dori, Z. *J. Am. Chem. Soc.* **1972**, *94*, 727–731.
(24) McFadden, D. L.; McPhail, A. T. *J. Chem. Soc., Dalton Trans.* **1974**, 363–366.
(25) Hussain, M. S.; Salinas, B. E. V.; Schlemper, E. O. *Acta Crystallogr.* **1979**, *B35*, 628–633.
(26) (a) Williams, D. E.; Wohlauer, G.; Rundle, R. E. *J. Am. Chem. Soc.* **1959**, *81*, 755–756. (b) Chakravorty, A. *Coord. Chem. Rev.* **1974**, *13*, 1–46.

N–O distance.[13,23,27] N–O (oxime) distances in the present three structures fall into three obvious sets.

(a) Long N–O Distances. These are observed for the protonated N–O bonds of (**1**) (N(1)–O(1) = 1.377 (5) Å), the protonated N–O bonds of (**3**) (N(2b)–O(2b) = 1.367 (5) Å and N(3b)–O(3b) = 1.372 (5) Å) and each of the protonated N–O bonds on the chloride-bridged side of **2** (N(2)–O(2) = 1.372 (4) Å and N(4)–O(4) = 1.374 (3) Å).

(b) Short N–O Distances. These are observed for the nonprotonated N–O bonds of (**1**) (N(2)–O(2) = 1.292 (5) Å) and **3** (N(1b)–O(1b) = 1.319 (5) Å and N(4b)–O(4b) = 1.308 (5) Å).

(c) Intermediate N–O Distances. These are observed only for the compressed N–O--H--O–N system of **2** in which N(1)–O(1) = 1.342 (3) Å and N(3)–O(3) = 1.333 (3) Å with associated O–H distances of O(3)–H(3) = 1.07 (5) Å and O(1)–H(3) = 1.44 (5) Å.

(3) Ru–N(glyoxime) Distances. The Ru–N distances in complexes **1–3** show substantial variations, ranging from 2.008 (3) to 2.079 (2) Å. All are shorter than the average Ru–N distance of 2.102 (6) Å observed in the related complex *trans*-[Ru(bpy)$_2$(NO)Cl](ClO$_4$)$_2$.[28] A similar shortening of Ru–N bonds was also observed in the macrocyclic complex *trans*-[Ru([14]-aneN$_4$)Cl$_2$]Cl, where short Ru–N bonds were believed to reflect the small cavity size of the cyclam ligand.[29]

In complexes **1–3**, the Ru–N distances are related to the N–O distances, which are, in turn, related to the protonation or nonprotonation of oxygen. Complexes **1** and **3** have their shorter Ru–N bonds associated with the protonated side of the oxime; thus Ru(1)–N(1) = 2.008 (3) Å for **1** and Ru(1b)–N(2b) = 2.010 (4) Å and Ru(1b)–N(3b) = 2.019 (4) Å for **3**. These are all shorter than Ru–N bonds on the nonprotonated side of the ligand, where Ru(1)–N(2) = 2.050 (3) Å for **1** and Ru(1b)–N(1b) = 2.039 (4) Å and Ru(1b)–N(4b) = 2.039 (4) Å for **3**.

For complex **2** the diprotonated dioxime bridge is associated with lengthened Ru–N bonds—Ru(1)–N(2) = 2.079 (2) Å and Ru(1)–N(4) = 2.079 (2) Å, while the compressed dioxime bridge yields Ru–N distances intermediate between the protonated and nonprotonated sides of **1** and **3**. Thus, in **2** we have Ru(1)–N(1) = 2.028 (2) Å and Ru(1)–N(3) = 2.032 (2) Å.

(4) The Equatorial N$_4$ Coordination Plane and the Chelate Rings. The four equatorial nitrogen atoms are coplanar to within ±0.02 Å for **1**, ±0.002 Å for **2**, and ±0.014 Å for **3**. The ruthenium atom is displaced from this plane (toward the nitrosyl ligand) by 0.175 Å in **1**, 0.155 Å and **2**, and 0.104 Å in **3**. In addition, the angle between the planes of the two glyoxime units in complex **1** is α = 18.2°; this changes to α = 19.9° for **2** and α = 7.7° for **3**. For comparison, we note that in Rh(DMGH)$_2$(PPh$_3$)Cl the rhodium atom is 0.126 Å from the four-nitrogen plane with α = 17.1°.[30]

The N–Ru–N bond angles associated with the five-member chelate rings of the N=C—C=N moiety are 77.6 (1), 76.0 (1), and 77.7 (1)° for complexes **1–3**, respectively. The deviations of the N–Ru–N bond angles from 90° are consistent with data obtained for other complexes that contain five-membered chelate rings and have been suggested to be dependent on the number of atoms in the chelate ring.[29] The rigidity of the equatorial dioxime angles associated with the N=C—C=N units for complexes **1** and **2** correspond closely to the values obtained for the uncoordinated dimethylglyoxime ligand and for transition metal complexes containing dimethylglyoxime or diphenylglyoxime.[27,31–33]

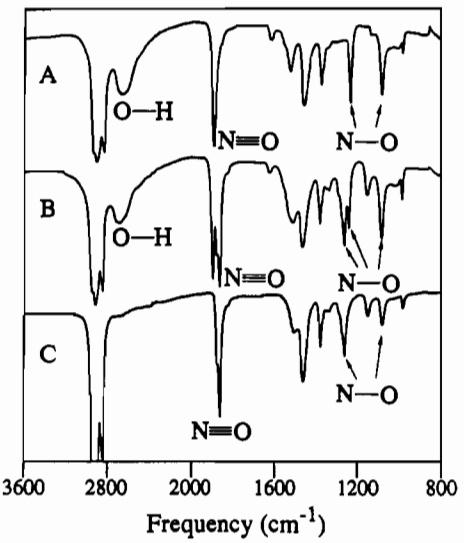

Figure 11. Infrared spectra of (a) *trans*-[Ru(DMGH)(DMGH$_2$)(NO)Cl)](Cl), (b) *trans*-[Ru(DMGH)(DMGH$_2$)(NO)Cl]Cl after heating in a vacuum oven overnight at 80 °C, and (c) *trans*-[Ru(DMGH)(DMGH$_2$)(NO)Cl]Cl after heating in a vacuum oven for a few days at 80 °C.

Thus protonation does not appear to effect the bite angle of the dioxime ligand.

(5) The Ruthenium–Nitrosyl and Ruthenium–Chloride Linkages. Among other noteworthy details offered by the structural determinations are values obtained for the bond lengths and angles associated with the *trans*-oriented nitrosyl and chloride ligands. The Ru–N and N–O bond lengths (1.749 (5) and 1.134 (7) Å for complex **1**, 1.756 (2) and 1.132 (3) Å for **2**, and 1.750 (3) and 1.134 (5) Å for **3**) are similar to those found for *trans*-[Ru(bpy)$_2$(NO)Cl](ClO$_4$)$_2$ (1.751 (6) and 1.132 (9) Å).[28] In addition, the Ru–Cl distances of 2.309 (2) and 2.314 (1) Å for complexes **1** and **2**, respectively, are also comparable to the value of 2.306 (2) Å obtained for *trans*-[Ru(bpy)$_2$(NO)Cl](ClO$_4$)$_2$.[28] Finally, the Ru–N–O angle associated with the nitrosyl ligand (180.0 (1)° for complex **1**, 179.7 (3)° for **2**, and 175.9 (3)° for **3**) confirms the presence of a linear nitrosyl (formally NO$^+$) ligand. Thus, no significant structural effects are imposed on the trans ligands by the equatorial dioxime ligands.

Infrared Spectroscopy. Although a number of single-crystal X-ray structures of transition metal glyoximes have been reported,[1,23–27,33] only a few of these structural determinations included the refinement of hydrogen atoms.[17,23–25] Thus, IR spectroscopy has been the primary characterization method regarding the protonation of *trans*-bis(dioxime) transition metal complexes, where structural assignments were made on the basis of characteristic N–O and O–H stretching frequencies.[12–15,34–36]

Wilkinson was the first to propose, on the basis of IR data, that protonation of cobaloxime complexes did not lead to an acid salt or lattice proton but instead resulted in the protonation of a hydrogen-bridged oxime oxygen.[12] Crumbliss studied the IR spectra of a number of cobaloximes of the general formula Co(DMGH)(DMGH$_2$)(X)(Y), where X and Y represent various anionic ligands, and compared their IR spectra with the IR spectra of the analogous nonprotonated complexes.[13,14] He reported that the solid-state IR spectra of the Co(DMGH)(DMGH$_2$)(X)(Y)

(27) Raston, C. L.; Skelton, B. W.; White, A. H. *Aust. J. Chem.* **1980**, *33*, 1519–1528.
(28) Nagao, H.; Nishimura, H.; Funato, H.; Ichikawa, Y.; Howell, F. S.; Mukaida, M., Kakihana *Inorg. Chem.* **1989**, *28*, 3955–3959.
(29) Walker, D. D.; Taube, H. *Inorg. Chem.* **1981**, *20*, 2828–2834.
(30) Cotton, F. A.; Norman, J. G. *J. Am. Chem. Soc.* **1971**, *93*, 80–84.
(31) Bruckner, S.; Randaccio, L. *J. Chem. Soc., Dalton Trans.* **1974**, 1017–1023.
(32) Bresciani-Pahor, N.; Calligaris, M.; Randaccio, L. *Inorg. Chim. Acta* **1978**, *27*, 47–52.
(33) (a) Bresciani-Pahor, N.; Forcolin, M.; Marzilli, L. G.; Randaccio, L.; Summers, M. F.; Toscano, P. J. *Coord. Chem. Rev.* **1985**, *63*, 1–125. (b) Lopez, C.; Alvarez, S.; Solans, X.; Font-Altaba, M. *Inorg. Chem.* **1986**, *25*, 2962–2969.
(34) Burger, K.; Ruff, I.; Ruff, F. *J. Inorg. Nucl. Chem.* **1965**, *27*, 179–190.
(35) Caton, J. E.; Banks, C. V. *Inorg. Chem.* **1967**, *6*, 1670–1675.
(36) Blinc, R.; Hazdi, D. *J. Chem. Soc.* **1958**, 4536–4540.

complexes contained three absorptions due to O–H stretches. Specifically, for the complex *trans*-Co(DMGH)($DMGH_2$)-(CH_3)Cl, he assigned the absorption at 3200 cm^{-1} to a non-hydrogen-bonded hydroxyl group, the absorption at 2575 cm^{-1} to an O–H--Cl intermolecular hydrogen bond, and the absorption at approximately 1700 cm^{-1} to an O–H--O intramolecular hydrogen bond.[13]

On the basis of the fact that the locations of the hydrogen atoms can be determined from the crystal structures of complexes **2** and **3**, we assign the IR absorbance at 2680 cm^{-1} for complex **2** to an intramolecular O–H--Cl hydrogen bond. The assignment of the 2680-cm^{-1} absorption band to an O–H--Cl intramolecular bond for complex **2** is further supported by the observation that this absorbance does not appear in the IR spectrum of complex **3** (see Figure 11).

For *trans*-bis(dioxime) transition metal complexes, the O–H stretch due to the O–H--O intramolecular hydrogen bridge typically is observed in the 1600–1800-cm^{-1} region.[13,35,36] The IR spectrum of complex **2** contains a weak absorption at 1615 cm^{-1}. We assign this absorbance to the O–H--O intramolecular hydrogen bridge. In complex **3** this absorbance disappears. The band most likely becomes too broad and weak to be observed.

The IR absorbances due to the N–O stretches for the dimethylglyoxime ligands are located at 1260 and 1080 cm^{-1} for complex **3**, while for complex **2** the higher N–O absorbance shifts to 1235 cm^{-1} (Figure 11). Upon protonation of similar cobaloxime complexes, Crumbliss reports a decrease in the higher (5–30 cm^{-1}) and lower (10–25 cm^{-1}) energy absorptions due to the N–O stretches.[13] The shift of N–O absorbances to lower energy is consistent with the protonation occurring at a hydrogen-bridged oxime oxygen atom, yielding a covalent O–H bond. The formation of an O–H bond results in the removal of electron density from the N–O bond and a corresponding increase in the N–O bond length and a decreased N–O stretching frequency. The proposed increase of an N–O bond length upon the formation of a covalent O–H bond associated with oxime oxygen has been confirmed by X-ray structural determination of complex **2**. Thus we have unambiguously extended the IR interpretation for cobalt complexes by Crumbliss to ruthenium *trans*-bis(dioxime) complexes.

The N≡O absorbance of the nitrosyl ligand coordinated to the ruthenium center is observed at 1860 cm^{-1} for complex **3** and at 1895 cm^{-1} for complex **2** (Figure 11). The 35-cm^{-1} increase of the N≡O absorbance upon protonation of complex **3** suggests that protonation of the dioxime ligand induces a decrease in the electron density at the ruthenium metal center.

^{1}H NMR Spectroscopy. The room-temperature ^{1}H NMR spectrum of complex **2** has been conducted in $(CD_3)_2SO$, where a broad singlet at 13.5 ppm and a singlet at 2.4 ppm with an integrated ratio of 1:6 was observed.[18] By analogy to other *trans*-bis(dimethylglyoxime) transition metal complexes these signals were assigned to the methyl protons and the bridging oxime protons respectively.[18]

The resonance for the two equivalent bridging oxime hydrogens of complex **3** appears at 11.6 ppm, while for complex **2** the resonance for the single bridging hydrogen occurs at 17.7 ppm. The increase in the chemical shift for the proton bridge in complex **2** as compared to complex **3** is believed to be a result of an increase in the strength of the hydrogen bond associated with the bridging proton. The increase in chemical shift as a function of increasing hydrogen bond strength has been previously observed for transition metal oxime complexes.[15] The proposed increase in the hydrogen bonding of the bridging proton in association with the protonated *trans*-bis(dimethylglyoxime)ruthenium complex has been demonstrated by the comparison of the X-ray crystallographic data for complexes **2** and **3**.

We conducted variable-temperature ^{1}H NMR experiments in CD_2Cl_2 of complex **2**. At −70 °C the ^{1}H NMR spectrum of complex **2** displays singlets at 2.4 and 2.5 ppm, which are assigned to the methyl protons of the dimethylglyoxime ligands, and singlets at 12.9 and 17.7 ppm, which correspond to the nonbridging oxime hydrogens and the symmetrically bridging oxime hydrogen, respectively. The inequivalence of the protons associated with the oxime oxygen atoms and methyl groups of complex **2** is consistent with the formulation as *trans*-[Ru(DMGH)($DMGH_2$)(NO)Cl]Cl. At temperatures above −70 °C extensive broadening of the oxime hydrogens and coalescence of the methyl protons is observed and attributed to proton exchange between the oxime hydrogens.

Table VIII. Rate Constants of Proton Exchange for [Ru(DMGH)($DMGH_2$)(NO)Cl]Cl in Dichloromethane

T, °C	k, M s^{-1}	T, °C	k, M s^{-1}
−40	30	25	750
−10	120	35	1550
18	500		

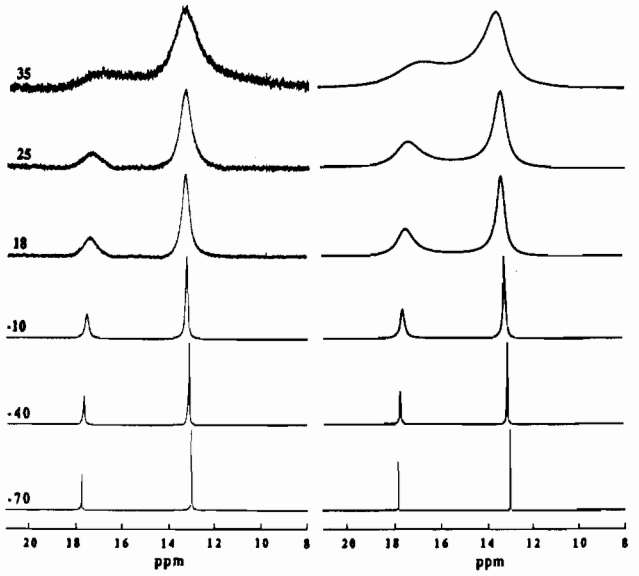

Figure 12. Experimental and calculated variable-temperature ^{1}H NMR spectra for the *trans*-[Ru(DMGH)($DMGH_2$)(NO)Cl]Cl complex.

^{1}H NMR spectra of **2** were collected at various temperatures, and a complete line shape analysis of the oxime hydrogen resonances was performed. Spectra were recorded at −40, −10, +18, +25, and +35 °C. The calculated rate constants are listed in Table VIII, and the experimental and calculated spectra are shown in Figure 12. The value of the free energy of activation, E_a (31 ± 7 kJ/mol), was calculated from an Arrhenius plot. In addition the values of ΔH^* (27 ± 8 kJ mol^{-1}) and ΔS^* (−96 ± 30 kJ mol^{-1} K^{-1}) were determined from an Eyring plot.[37] Due to the limitations of dynamic NMR line shape analysis no interpretations of the ΔH^* and ΔS^* values will be made.[37,38]

The proposed exchange mechanism for this system is a two to one exchange, where the nonbridging hydrogens exchange with the symmetrically bridging oxime hydrogen. Bridging (O–H--O) protons of cobaloxime complexes have been shown to undergo rapid exchange with free water.[39] Since there is no detectable free water resonance in the ^{1}H NMR spectra of **2**, the probability of such an exchange is low. Proton exchange between complex **2** and the solvent is also possible. However, since the resonance at δ = 5.32 does not appear to broaden as the temperature is increased, such an exchange is probably not occurring.

To determine the effect of ruthenium concentration on the rate of proton exchange, spectra were recorded at three different concentrations of ruthenium (0.026, 0.020, and 0.011 M *trans*-[Ru(DMGH)($DMGH_2$)(NO)Cl)]Cl) and the rate of exchange vs concentration of **2** was plotted. There appears to be no dependence of the rate on the concentration of **2**; therefore, the exchange rates reported here represent a purely intramolecular

(37) Sandstrom, J. *Dynamic NMR Spectroscopy*; Academic Press: New York, 1982.
(38) Binsch, G.; Kessler, H. *Angew. Chem., Int. Ed. Engl.* **1980**, *19*, 411–494.
(39) (a) Guschl, R. J.; Brown, T. L. *Inorg. Chem.* **1974**, *13*, 959–965. (b) Brown, T. L.; Ludwick, L. M.; Stewart, R. S. *J. Am. Chem. Soc.* **1972**, *94*, 384–393.

hydrogen exchange (zero-order kinetics).[40]

The ^{1}H NMR spectrum of complex **2** conducted at −70 °C is the first example of an ^{1}H NMR spectrum of a protonated *trans*-bis(dioxime) transition metal complex which demonstrates the inequivalence of the protons associated with the oxime oxygens and the methyl groups. From this data we conclude that the proposed solid-state structure is maintained in solution.

The variable-temperature ^{1}H NMR experiments demonstrate that the proton exchange occurs at room temperature. The existence of proton exchange may therefore explain the lack of detection of oxime protons for other protonated *trans*-bis(dioxime) transition metal complexes.

Cyclic Voltammetry. For complex **3** a reversible couple ($i_{p,c}/i_{p,a}$ = 1.0) is present with $E_{1/2}$ = −0.27 V (CH_2Cl_2, V vs SSCE) which corresponds to the $[Ru(DMGH)_2(NO)Cl]^{0/-}$ couple. The potential of the analogous couple for complex **2**, $E_{1/2}$ = −0.03 V (CH_2Cl_2, V vs SSCE), occurs at a potential 240 mV more positive than that for complex **3**. The shift of the reduction couple to a more positive potential is consistent with a decrease in the electron density at the ruthenium center upon dioxime protonation, which is in agreement with our interpretation of the IR shift in the N≡O stretching frequency. Similar potential shifts were observed for ruthenium complexes containing an benzil oxime ligand and were attributed to the protonation of the oxime ligand.[41]

Dissociation Constants. A potentiometric titration of *trans*-[Ru(DMGH)(DMGH$_2$)(NO)Cl]Cl **2** was performed and pK_a values of 3.38 ± 0.10 (pK_{a1}) and 5.26 ± 0.17 (pK_{a2}) were measured for the removal of two protons. A potentiometric titration was also performed on *trans*-$[Ru(DMGH)_2(NO)Cl]$ (**3**) (pK_a = 5.14 ± 0.17), and the titration curve obtained was identical to the titration curve obtained for **2** in the region pH = 4.00–10.00. The complex $H[Co(DMGH)_2(Cl)_2]$, which we would formulate as $Co(DMGH)(DMGH_2)(Cl)_2$, has reported pK_a values of approximately 3.4 and 6.7.[42] Other cobalt complexes such as $RCo(DMGH)(DMGH_2)L$ (R = Me, Et, and *i*-Pr and L = H_2O or R = alkylperoxy and L = H_2O, NH_3, pyridine, and piperidine) have pK_{a1} values between 0–1.0 and complexes such as $[Co(DH)_2L_2]^+$ (where DH = monoanion of various dioxime ligands and L = pyridine, aniline, and various pyridine and aniline derivatives) have pK_a values ranging from 6.0 to 10.8.[9,43,44]

The axial ligands of the $[Co(DH)_2L_2]^+$ complexes effect the acidity of the oxime protons.[43,44] Complexes with axial pyridine derivatives are stronger acids than those with axial aniline derivatives. Yamano explained this trend by proposing that the $d\pi(d_{xz}d_{yz})$–$p\pi$(pyridine) interaction stabilizes the $d\pi$-orbitals while weakening the $d\pi(d_{xz},d_{yz})$–$p\pi$(oxime) bonding which removes electron density from the oxime oxygen atoms.[44,45] Since pyridine is a better π acid than aniline, the interaction is favored, and complexes with axial pyridine derivatives are stronger acids than those with axial aniline derivatives.

The pK_a values for the $[Co(DH)_2L_2]^+$ complexes are higher than that of *trans*-$[Ru(DMGH)_2(NO)Cl]$ (**3**). On the basis of the axial ligand trends mentioned above, we attribute this to the axial nitrosyl ligand, which is a better π acid than pyridine or aniline. Since it is a better π acid, it can better stabilize the negative charge on the oxime oxygen atoms, therefore making *trans*-$[Ru(DMGH)_2(NO)Cl]$ a stronger acid than $[Co(DH)_2L_2]^+$.

Acknowledgment. This work was supported in part by the National Science Foundation (Grant CHE 8814638), the donors of the Petroleum Research Fund, administered by the American Chemical Society, and the ARCO Chemical Co. Purchase of the X-ray diffractometer was made possible by Grant 89-13733 from the Chemical Instrumentation Program of the National Science Foundation. We also thank Dr. Jerome B. Keister for his useful discussions regarding dynamic NMR spectroscopy and for the use of the DNMR3 program and Johnson Matthey Inc. for their generous loan of $RuCl_3 \cdot 3H_2O$.

Registry No. **1**, 110340-75-5; **2**, 138694-43-6; **3**, 110340-76-6.

Supplementary Material Available: Complete tables of bond lengths, bond angles, anisotropic thermal parameters, and calculated hydrogen parameters for *trans*-$Ru(DPGH)_2(NO)Cl$ (**1**), *trans*-$[Ru(DMGH)(DMGH_2)(NO)Cl]Cl$ (**2**), and *trans*-$Ru(DMGH)_2(NO)Cl$ (**3**) (9 pages); list of F_o/F_c for **1**–**3** (38 pages). Ordering information is given on any current masthead page.

(40) (a) Pearson, R. G.; Anderson, M. *Angew. Chem., Int. Ed. Engl.* **1965**, *4*, 281–287. (b) Zumdahl, S. S.; Drago, R. S. *J. Am. Chem. Soc.* **1967**, *89*, 4319–4322.
(41) Chakravarty, A. R.; Chakravorty, A. *J. Chem. Soc.* **1982**, 1765–1771.
(42) Costa, G.; Tauzher, G.; Puxeddu, A. *Inorg. Chim. Acta* **1969**, *3*, 45–48.
(43) Espenson, J. H.; Chen, J.-T. *J. Am. Chem. Soc.* **1981**, *103*, 2036–2041.
(44) Yamano, Y.; Masuda, I.; Shinra, K. *J. Inorg. Nucl. Chem.* **1971**, *33*, 521–527.
(45) Yamano, Y.; Masuda, I.; Shinra, K. *Bull. Chem. Soc. Jpn.* **1971**, *44*, 1581–1585.